

Design and analysis of a novel claw-shaped modular stator relieving-DC-saturation doubly salient machine with 3D complementary magnetic circuit

Zhenghao Li  | Shuangxia Niu

Department of Electrical Engineering, The Hong Kong Polytechnic University, Hong Kong

Correspondence

Shuangxia Niu, Department of Electrical Engineering, The Hong Kong Polytechnic University, Hong Kong.

Email: eesxniu@polyu.edu.hk

Funding information

National Natural Science Foundation of China under Project 52077187; Research Grant Council of the Hong Kong Government under Project PolyU 152143/18E and PolyU 152109/20E.

Abstract

Here, a novel DC-excited doubly salient machine with a claw-shaped modular stator and three-dimensional (3D) complementary magnetic circuit is proposed for wind power generation application. The key is to artificially construct a 3D complementary structure to suppress torque ripple and employ auxiliary slot-opening PMs to relieve DC-saturation in the stator core and improve overload capability. The novel 3D complementary structure provides an alternative magnetic path for the main flux, so the flux leakages in the air gap at open-circuit position are effectively cancelled, and the flux in the yoke remains relatively constant. Hence, the output torque ripple is suppressed. Furthermore, the saturation issue in the stator is solved with auxiliary permanent magnets which have opposite magnetization direction to that of DC field excitation. Therefore, the torque capacity of the machine is improved. Here, the machine structure and operation principle are introduced, and a 2D equivalent model is also developed to replace the 3D model to improve the calculation efficiency. Multi-objective optimization algorithm is developed to improve the performance of this new machine. The validity of machine design is finally verified with 2D and 3D finite element analysis.

1 | INTRODUCTION

Due to overexploitation and consumption of energy, environmental pollution has been increasingly serious, and fossil fuels are running out. Therefore, it is urgent to find new renewable energy power generations to replace conventional fossil fuels, and wind power generation is the most popular and attractive technology [1, 2]. According to the operation speed and output voltage frequency, the wind-generation system can be categorized into two different types, namely, constant-speed constant-frequency (CSCF) and variable-speed constant-frequency (VSCF) wind harvesting system [3]. As the CSCF type wastes abundant mechanical power to keep speed constant, the system efficiency is rather low. In recent years, thanks to the development of power electronics, VSCF system with improved wind energy conversion capability has attracted more attention in the wind harvesting field.

As shown in Figure 1, VSCF wind harvesting basically consists of the following parts, which include blades, gear box, wind turbine, converters, and load. As one of the most critical parts in the wind power generation system, wind turbine should satisfy lots of criteria to achieve the energy conversion mission efficiently. The current development trend for wind turbine is to develop a generator with low cost, high reliability, high-power conversion efficiency, low torque ripple, good voltage-regulation ability, and high fault-tolerant capability etc.

Especially, with the fluctuating supply of rare earth materials and drastic increase in price of PM material, to improve product competitiveness, less permanent magnet or magnet-free machine becomes a new trend of wind generator design [4, 5]. Considering the drawbacks of PM-excited machines, researchers are shifting their attention back to DC-excited (DCE) machines. Among all kinds of DCE machines, DC-excited doubly salient machines (DCE-DSM), which have merits of good flux-regulation capability, high robustness, and low cost, are suitable for wind power generation application. In [6], a

This is an open access article under the terms of the [Creative Commons Attribution](https://creativecommons.org/licenses/by/4.0/) License, which permits use, distribution and reproduction in any medium, provided the original work is properly cited.

© 2021 The Authors. *IET Renewable Power Generation* published by John Wiley & Sons Ltd on behalf of The Institution of Engineering and Technology

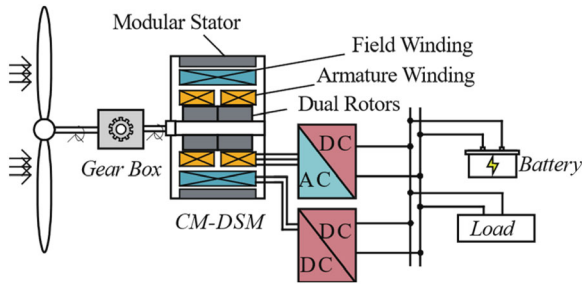


FIGURE 1 Schematic of wind power harvesting system with modular stator CM-DSM

DC-excited doubly fed doubly salient machine was proposed for wind harvesting system. However, the torque ripple is relatively large, and fault-tolerance capability still needs to be enhanced further.

To improve the robustness and reliability of DSMs and to facilitate the manufacturing process, modular stator doubly salient machines (MS-DSM), which separate the stator into several modules, are proposed [7–11]. In [7], a hybrid-excited modular stator DSM is proposed to extend the speed range. Benefiting from the modular stator design, the proposed machine is easy to manufacture, assemble, and maintain. Moreover, the hybrid excitation topology increased the power capability of this machine. However, this DSM suffers from higher-order harmonics of back EMF, which causes torque ripple and extra power loss in wind-power application, and the problem of unbalanced magnetic force (UMF), which may further cause vibration and noise. In [8], a modular stator switched reluctance machine (MS-SRM) which could accomplish fault-tolerance, high efficiency and high power density is designed. The torque ripple, however, has reached almost 40%, which greatly hindered the application of this machine. Therefore, due to the inherent weaknesses of structure, both modular stator machine and non-modular stator machine still suffer from problems such as high torque ripple and low torque density, which hinder the development of this kind of machine.

To address the torque ripple issue, complementary structures have been applied in different types of DSM [11–13]. In [11], a radial-flux machine with complementary structure is proposed, which is composed of an inner rotor and outer rotor. A disk doubly salient machine is proposed in [12], which adopts axial complementary structure. In the existing literatures, however, most of them focused on the 2D complementary structure, which involves two air gaps, and the complicated mechanical structure results in higher requirement for bearings and manufacturing accuracy.

To improve the torque density of machines with less permanent magnet or magnet-free DSM machines, researchers have investigated variable methods [3, 14, 15]. In [3], a dual-mode motor, which is excited by only DC winding, has been proposed to improve the output torque by adopting both doubly salient design and flux switching design in one machine. Apart from power electronics device to switch mode, this machine employed two sets of winding to realize the dual-mode oper-

ation, which makes the whole system quite complicated and redundant. In [15], high temperature superconductor (HTS) is employed to provide field excitation for DSM. However, for HTS excitation machine, a complicated cooling system is required, which increases its manufacturing cost and difficulties of the machine. Another method to improve the machine's torque density and increase the energy conversion capability is to solve the DC-component saturation issue in the machine. From this perspective, auxiliary PMs located at slot opening, which are named as slot opening, have been employed by researchers to relieve DC-saturation in the core [16].

In this paper, a novel claw-shaped modular stator doubly salient motor (CM-DSM) with complementary structure is proposed. The stator adopts modular stator design, which improves the fault-tolerant capabilities of machine. The combinations of claw-shaped stator and dual rotors construct a complementary structure artificially, which reduce the torque ripple of machine, and boost the output torque meanwhile. In addition, thanks to the 3D complementary structure, the two parts of the machine share one common air gap, which simplifies the mechanical structure. To further improve overload capability, the auxiliary PMs located at slot-opening is also employed in this machine to relieve the DC-saturation in the stator core. To simplify the calculation, 2D equivalent finite element (FE) model is developed to replace the 3D finite element model. Multi-objective optimization algorithm is also developed to further improve the performance of this new machine.

This paper is organized as follows: In Section 2, the topology and operation principle of this new design is demonstrated; methods and proof of simplified 2D equivalent FE model replacing 3D model are illustrated in Section 3. The configuration parameters of the model are optimized by the multi-objective optimization algorithm to improve the performance of this new machine in Section 4. Section 5 analyses the specific characteristics and performances of this novel machine. In Section 6, the electrical performance of the optimized model is compared with the conventional modular stator DSM using the finite element method (FEM), and the simulation results are verified by 3D model. Some conclusions are drawn in Section 7.

2 | MACHINE STRUCTURE AND OPERATION PRINCIPLE

2.1 | Machine structure

Due to the serious open-circuit flux leakage in conventional DSMs, the energy conversion capabilities of it are limited and the output torque of the machine is also affected, which may influence the quality of the power generation. In this paper, CM-DSM develops a 3D complementary structure to address the flux leakage issue of DSM.

Figure 2a shows the structure of the proposed machine and Figure 2b demonstrates the cross section of the machine. The proposed CM-DSM consists of 6 modular stator segments, which cut off the magnetic path connection between two different modules, and the rotor adopts 10 salient-tooth rotor poles,

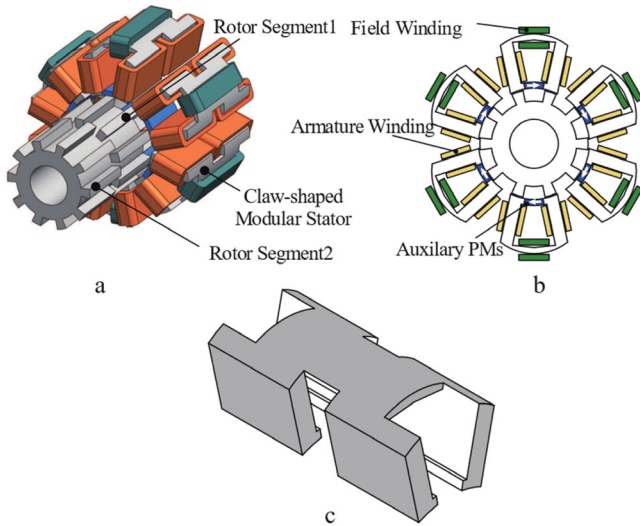


FIGURE 2 Configuration of proposed CM-DSM: (a) three-dimensional model, (b) cross section, and (c) claw-shaped modular stator

namely, a classic 12/10 slot/pole combination adopted in this machine. The rotor has two segments along the axis, between which the screw electrical angle shift is set as π . Each modular stator adopts claw-shaped design, which has 4 stator teeth with both DC windings and AC windings wound around. DC field coils are wound around the yoke of each module identically to provide a balanced DC excitation field for each module. The stack length of yoke is decreased artificially to reduce the copper loss of DC windings. Since the flux going through the armature windings is unipolar, tangential magnetized auxiliary PMs are installed at slot opening to relieve the DC-component flux in the core.

The design features of the proposed DSM can be summarized as follows:

1. The stator adopts claw-shaped modular design with 4 coils of AC concentrated winding wound around, which could improve the fault-tolerant capabilities of the machine and simplify the manufacture and the installation of the machine.
2. The rotor has two segments in the axial direction between which an electrical angle of π is switched. This artfully 3D axially complementary structure could realize the torque ripple suppression.
3. The PMs are installed at slot-opening of each module to provide a constant reversal flux to relieve DC-saturation issue, which could improve the torque production.

2.2 | Operation principle

As presented in Figure 2, the proposed generator accomplished a complementary structure along the axis. The 3D model is quite complicated. Therefore, in this section, the 3D complementary structure magnetic circuit of one module is simplified to a 2D model, which is shown in Figure 3.

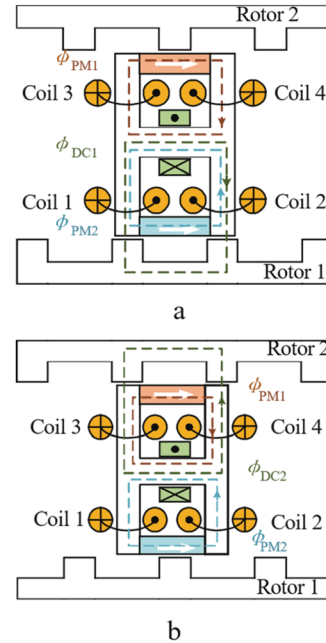


FIGURE 3 Illustration of flux distribution in CM-DSM

As denoted in Figure 3, when the rotor moves to position (a), where the lower rotor salient poles, which is denoted as Rotor 1, are aligned with the lower part of the modular stator, flux generated by DC windings would go through Coil 1, Rotor 1, and Coil 2 to form the loop, and the reluctance of the lower loop for DC excitation is minimized. Therefore, the flux in coil 1 and coil 2 reaches the top. The windings of this module are aligned with d axis at this position. On the other side, due to the large reluctance between the upper part of the modular stator and rotor 2, the flux going through Coil 3 and Coil 4 at this position reaches the minimum value. Vice versa, when the rotor moves to position (b), as shown in Figure 3b, the rotor rotates to the position where Rotor 2 aligned with the upper part of the modular stator, the flux in coil 3 and coil 4 reaches the top in opposite direction.

As shown in Figure 3, since the stator yoke provides a short-cut path, the flux linkages excited by the auxiliary PMs, namely, φ_{pm1} and φ_{pm2} , flow through the modular stator constantly and are always opposite to flux linkages generated by DC field winding. With slot PM desaturation effect, the DC-component of flux linkages, which makes no contribution to output torque, is relieved. In this way, the energy conversion capabilities of the machine, especially at heavy electrical load, could also be improved as well. With a continuous anti-clockwise rotation, the alignment between the modular stator teeth and rotor salient poles changes periodically, which makes it possible for the electro-mechanical energy conversion. Thanks to the complementary design, the flux leakages at the open-circuit position are effectively reduced, and the induced voltage generated by the effective flux linkages linking could be prompted as well. The validation of this will be presented in Section 5.

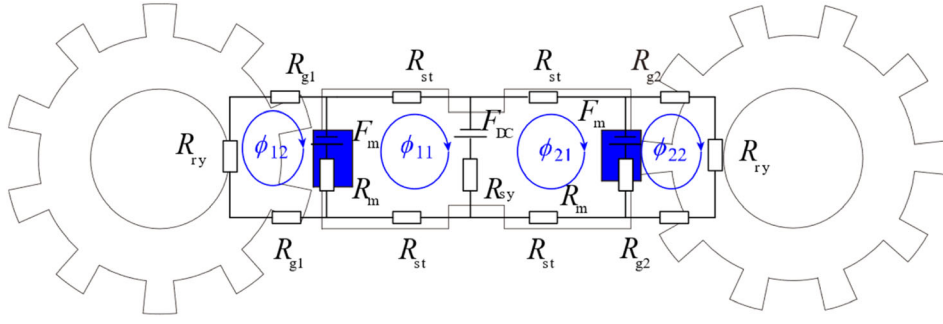


FIGURE 4 Magnetic circuit of the proposed machine

2.3 | Complementary magnetic circuit

Equivalent magnetic circuit (EMC) analysis is one of the most useful methods to simplify and analyse the static magnetic field in electrical machines. In this section, with the help of EMC analysis, the merits of the complementary structure of the proposed machine are demonstrated. The EMC model of one complementary-structure modular stator under no-load condition is shown in Figure 4. As shown in Figure 4, there are two symmetric magnetic return paths for the field DC winding excitation F_{DC} , and fluxes excited by both DC winding and PMs can also be solved using the loop current method, where F_{DC} and F_m are the magneto-motive force (MMF) of DC field winding and PMs, R_m is the internal reluctance of PM, R_{sy} and R_{st} are the reluctance of stator yoke and stator teeth, respectively, R_{ry} is the reluctance of rotor yoke, and R_{g1} and R_{g2} are the reluctance of air gap at both sides of the complementary stator, and the value of them is varied periodically according to the relative position between the rotor and stator.

where $R_1 = 2R_{st} + 2R_{g1} + R_{ry} + R_{sy}$; $R_2 = 2R_{st} + 2R_{g2} + R_{ry} + R_{sy}$. When the complementary structure is adopted, R_1 and R_2 could be divided into constant part and variable part and be rewritten as, $R_1 = R_0 + \Delta R$ and $R_2 = R_0 - \Delta R$, where R_0 represents the constant part of reluctance and ΔR represents the variable part ($\Delta R > 0$).

In this way, the difference between the maximum value of flux and the minimum value of flux $|\phi_{\max} - \phi_{\min}|$, which represents the amplitude of the fundamental components of flux linkage could be expressed as Equation (4).

On the contrary, when there is no complementary structure, it could be expressed as Equation (5). In this condition, R_1 equals to R_2 , which could be expressed as $R_{1,2} = R_0 \pm \Delta R$.

$$|\phi_{\max} - \phi_{\min}| = \frac{4\Delta R}{R_{sy}^2 - R_0^2 + \Delta R^2} F_{DC} \quad (4)$$

$$\begin{bmatrix} R_m + 2R_{st} + R_{sy} & -R_m & -R_{sy} & 0 \\ -R_m & 2R_{g1} + R_{ry} + R_m & 0 & 0 \\ -R_{sy} & 0 & R_m + 2R_{st} + R_{sy} & -R_m \\ 0 & 0 & -R_m & 2R_{g2} + R_{ry} + R_m \end{bmatrix} \begin{bmatrix} \phi_{11} \\ \phi_{12} \\ \phi_{21} \\ \phi_{22} \end{bmatrix} = \begin{bmatrix} F_{DC} - F_m \\ F_m \\ -F_{DC} + F_m \\ -F_m \end{bmatrix} \quad (1)$$

According to the loop current method, the main flux in the proposed generator ϕ_{11} , ϕ_{21} under no-load situation can be solved with Equation (1), which is further expressed as Equations (2) and (3).

$$\phi_{11} \approx -\frac{1}{R_m} F_m + \frac{R_{sy} - R_2}{R_{sy}^2 - R_1 R_2} F_{DC} \quad (2)$$

$$\phi_{21} \approx \frac{1}{R_m} F_m - \frac{R_{sy} - R_1}{R_{sy}^2 - R_1 R_2} F_{DC} \quad (3)$$

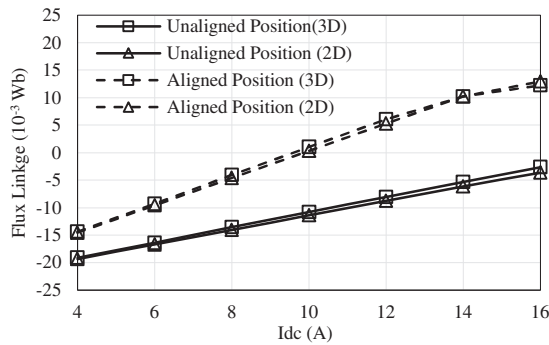
$$|\phi'_{\max} - \phi'_{\min}| = \frac{4\Delta R}{R_{sy}^2 - R_0^2 + 2R_{sy}R_0 + \Delta R^2} F_{DC} \quad (5)$$

Comparing Equations (4) and (5), it could be found that, due to the complementary structure, the amplitude of the fundamental components of flux linkage is boosted, namely, the reluctance torque of the proposed machine could be improved under the same magnetic load.

Besides, when the complementary structure is adopted, flux going through the stator yoke at short-circuit position could be

TABLE 1 Machine parameters relationships

Symbol	Relationship
g'	$r_{s0} \ln(r_{r0}/r_{s0} - g)$
w'_{rt}	$r_{s0} \alpha_{rt}$
b'_{rt}	$r_{s0} \ln(r_{r0}/r_{s0} - b_{rt})$
b'_{ry}	$2b_{ry}$
w'_{st}	$r_{s0} \alpha_{st}$
w'_{sy}	$r_{s0} \alpha_s$
b'_{st}	b_{st}
b'_{sy}	$2b_{sy}$
w'_{pm}	$r_{s0} \alpha_{pm}$
b'_{pm}	b_{pm}

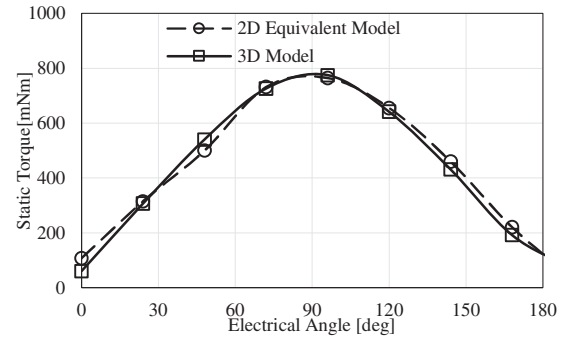
**FIGURE 6** Static flux linkages under different current

where φ_m is flux linkage provided by PM, Λ_m is inner permeance of PMs, and variables with/without prime represent the parameters of the 2D/3D model.

According to Equation (10), when the constant MMF F_c and inner reluctance of PMs remain unchanged, the equivalence of PMs is guaranteed. To satisfy the principles above, the parameters of 2D and 3D model should obey the relationships which are listed in Table 1.

3.2 | Comparison of 2D and 3D FE Model

To verify the validation of the equivalent method proposed above, the static performances of 3D and 2D equivalent model, including main flux linkages and static angle-torque characteristics, are compared with Ansys Maxwell software, which is presented in Figures 6 and 7. Figure 6 presents the flux linkages of one module at aligned position and unaligned position under no-load condition. The DC field excitation current varies from 1 A to 12 A, which simulates the equivalent effect under different saturation condition. Figure 7 presents the static torque of two models, when the excitation current is fixed as 4A. It could be found that the two models agree well with each other in the static performance indicating that the 2D equivalent model replaced the 3D model properly.

**FIGURE 7** Static angle-torque characteristic**TABLE 2** Optimal range of main parameters

Symbol	Main parameter	Unit	Range
α_{st}	Angle of stator teeth	deg	11–15
α_s	Angle between two teeth of the stator	deg	16–24
b_{pm}	Height of Slot PM	mm	2–4
ratio1	Split ratio between r_{s0} and r_{s1}	–	0.4–0.6
ratio2	Split ratio between α_{st} and α_{rt}	–	0.75–1.25
ratio3	Split ratio between α_{pm} and α_s	–	0.7–0.95
N_{dc}	Turns of DC winding	–	100–200

4 | DESIGN OPTIMIZATION

In this section, to improve the energy conversion capability of the proposed generator, the output torque of the machine and torque ripple of it are optimized simultaneously, and multi-objective genetic algorithm (MOGA) is applied to determine the optimized configuration parameters of the proposed machine. 2D equivalent linear model, whose effectiveness has been verified in the previous section is applied to the optimization process instead.

4.1 | Parameters analysis

The optimal configuration parameters which have a significant influence on objectives are defined as main parameters. In this part, some main parameters of the proposed machine are identified and optimized, which are presented in Table 2 and Figure 8. In Table 2, the main parameters and optimal range are defined.

Figure 8a presents the effect of α_s on the machine's output torque and torque ripple. It could be found that α_s has significant effect on the torque and torque ripple. Figure 8b shows the influence of split ratio on the machine's output torque and torque ripple. As the split ratio increases, the output torque rises, however, the torque ripple of the machine increases at the same time. Figure 8c demonstrates the relationship between the turns of DC windings and the electromagnetic performance of the machine. It can be found that when the turns of AC coils and DC coil are approximately separated equally, the maximum out-

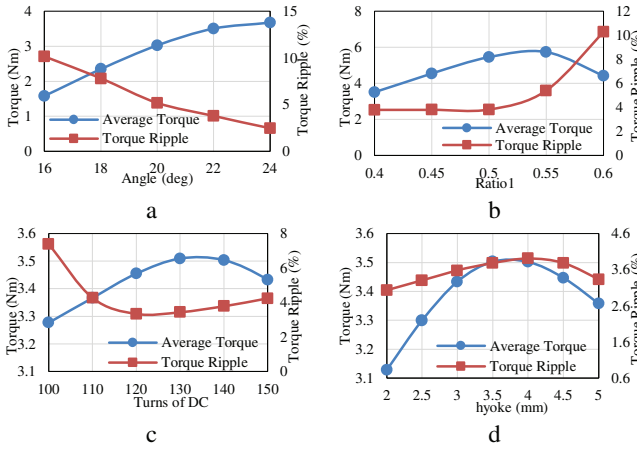


FIGURE 8 Parameter analysis of CM-DSM: (a) α_s , (b) split ratio, (c) turns of DC, (d) h_{yoke}

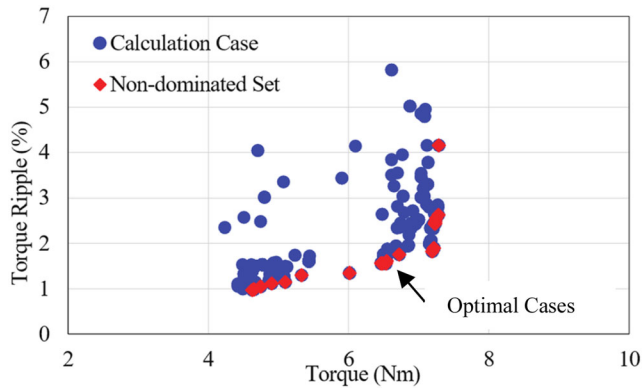


FIGURE 9 Optimization results of the proposed CM-DSM

put torque could be achieved. Figure 8d describes the effect of the height of stator yoke on the performance of the machine.

4.2 | Optimization results

According to the parameter analysis above, it could be found that the targets of torque maximization and torque ripple minimization could not be reached simultaneously. Therefore, the optimization front of the CM-DSM, which integrates two objectives, is derived after 40 generations of iteration of MOGA, as presented in Figure 9. The number of individuals in each iteration generation is set as 40. The parameters of the initial design are presented in Table 3.

It could be found that the torque of the proposed machine could achieve approximately 6.2 Nm, and torque ripple could be reduced to as low as 6%. An optimal case which achieves both high torque and low torque ripple, as shown in Figure 9, is picked up for further analysis. The specific parameters of the optimal design are summarized and listed in Table 4. The major materials of the proposed machine are listed in Table 5.

TABLE 3 Initial design parameters of CM-DSM machine

Symbol	Parameter	Unit	Value
α_{st}	Angle of stator teeth	deg	11
α_s	Angle between two teeth of stator	deg	22
h_{st}	Height of stator teeth	mm	32.5
h_{sy}	Height of stator yoke	mm	3.5
G	Length of air gap	mm	0.5
r_{out}	Outer radius of the machine	mm	60
r_0	Radius of the inner rotor	mm	12.5
h_{ry}	Height of rotor yoke	mm	8
h_{rt}	Height of rotor teeth	mm	5.5
α_{rt}	Angle of rotor teeth	deg	12
h_{pm}	Height of PM	mm	2.5
α_{pm}	Angle of PM	deg	19.8
N_{dc}	Turns of DC coil of one module	–	140
N_{ac}	Turns of one AC coil	–	70
I_{dc}	Current of DC winding	A	10
I_d	D-axis current	A	0
I_q	Q-axis current (rms)	A	10

TABLE 4 Optimized parameters of CM-DSM machine

Symbol	Parameter	Unit	Initial	Optimal
α_{st}	Angle of stator teeth	deg	11	11.35
α_s	Angle between two teeth of stator	deg	22	25
h_{pm}	Height of Slot PM	mm	2.5	4.12
ratio1	Split ratio	–	0.4	0.448
ratio2	Ratio between α_{st} and α_{rt}	–	0.9	0.812
ratio3	Ratio between α_{pm} and α_s	–	0.9	0.949
N_{dc}	Turns of DC winding	–	140	112

5 | PERFORMANCE EVALUATION AND COMPARATIVE STUDY

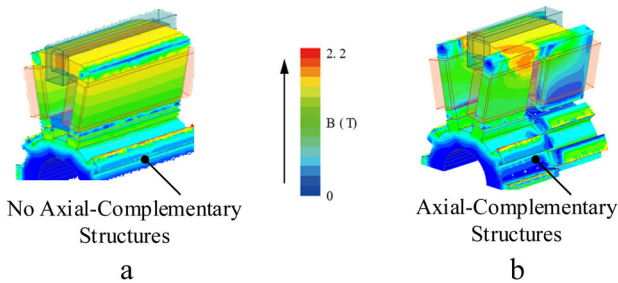
In this section, the electromagnetic performance of the proposed CM-DSM, including its flux distribution, voltage characteristics, torque characteristics, and fault-tolerance capability, is evaluated. The performance of the machine with 3D complementary structure is compared with a conventional MS-DSM machine without 3D complementary structure to illustrate the effectiveness of the proposed complementary structure.

5.1 | Open-circuit performance

Figure 10 demonstrates the flux distribution of both conventional MS-DSM and the CM-DSM proposed in this paper

TABLE 5 Materials of proposed machine

Material	Specification	Value
PMs	Type	NdFeB30
	Br	1.1T
	Coercive force	838 kA/m
Steel	Type	JFE_Steel_35
	Saturated point	1.7T
Winding	Conductivity	5.8×10^7 S/m

**FIGURE 10** Flux distribution in 3D model

at aligned position. With 12/10 slot/pole combination, the machine is symmetric. Thus, only half of the model is built.

Different from MS-DSM shown in Figure 10a, with claw-shaped complementary magnetic path design, the flux linkages generated by DC winding passing air gap are always linking with the two rotors regardless of the position of the rotor. Therefore, the air gap flux leakages are reduced, and the main flux is strengthened as well. On the other hand, the flux linkages in the yoke remain constant.

Figure 11 presents the flux linkage distribution in both armature winding (Figure 11a) and yoke (Figure 11b) when DC-excitation current is set as 4A and 10A, respectively. It is found in Figure 11a that different from the conventional MS-DSM, flux linkages in CM-DSM are bipolar. As the current increases from 4A to 10A, the amplitude of the flux linkages increases as well in CM-DSM, whereas the increasing current only brings more DC-saturation in the conventional MS-DSM machine. Figure 11b illustrates that the flux linkages in the yoke of conventional MS-DSM vary a lot, while those of CM-DSM machines remain relatively constant.

Using the method of fast Fourier transformation (FFT) analysis, the flux linkages spectra of both conventional MS-DSM machine and the proposed CM-DSM machine are illustrated in Figure 12. In accordance with the analysis above, Figure 12 shows that the fundamental component of flux linkage of machine with 3D complementary structure are higher than those of machine without 3D complementary structure, when the current is set as 10 A. In addition, though it has been proved in [7] that flux linkages of machines with 10 rotor poles have higher even-order harmonics, thanks to the 3D complementary structure, CM-DSM machine with 12/10 stator/rotor poles combination eliminated the even-order harmonics in flux linkages completely.

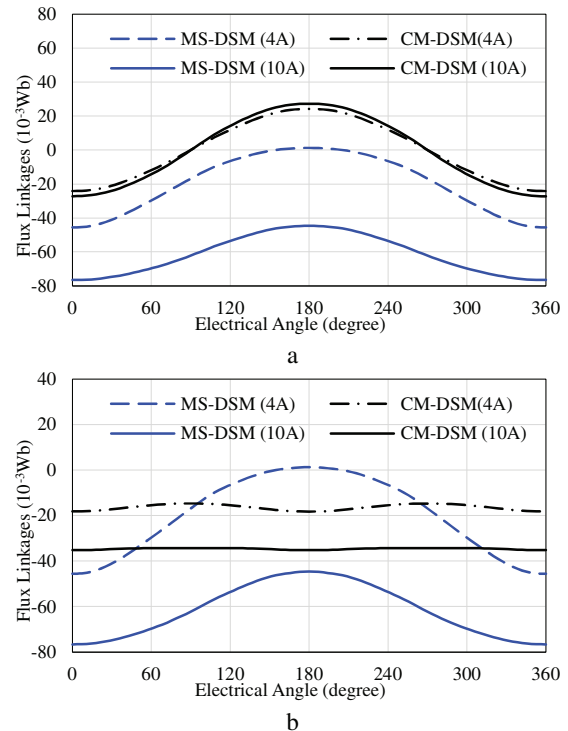
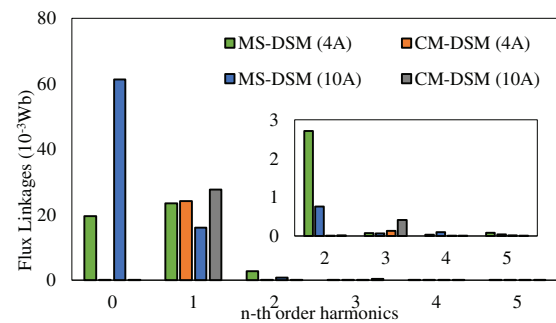
**FIGURE 11** Flux linkages comparison: (a) armature-winding flux linkages, (b) yoke flux linkages**FIGURE 12** Flux linkages harmonics in CM-DSM and MS-DSM

Figure 13a presents induced voltage in one phase generated by CM-DSM and MS-DSM at a speed of 1200 rpm. Figure 13b presents the rectified voltage of the proposed machine after full-bridge rectification. It could be found that the proposed machine has better voltage-regulation capability: due to better desaturation capabilities of CM-DSM, its output voltage has wider range at the same excitation and speed comparing with conventional MS-DSM. Moreover, comparing with the conventional MS-DSM, the machine with the proposed structure has more stable output voltage after full-bridge rectification.

5.2 | Torque characteristics comparison

Torque characteristics represent energy conversion capability of the proposed generator, which is critical in power generation

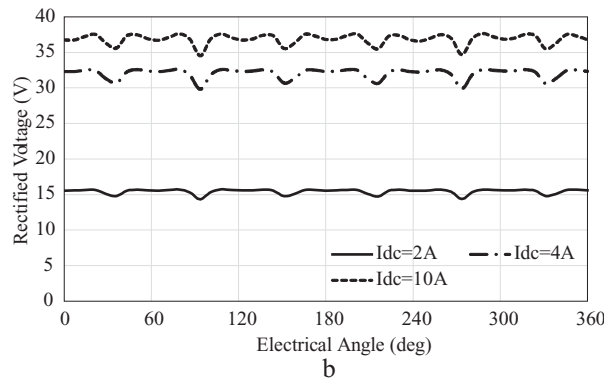
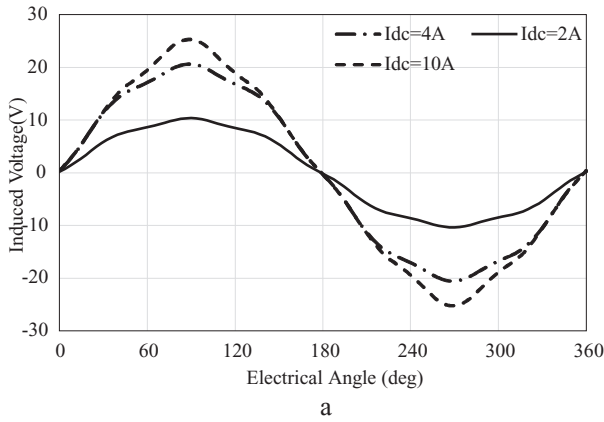


FIGURE 13 Induced voltage of one phase: (a) induced voltage, (b) rectified voltage

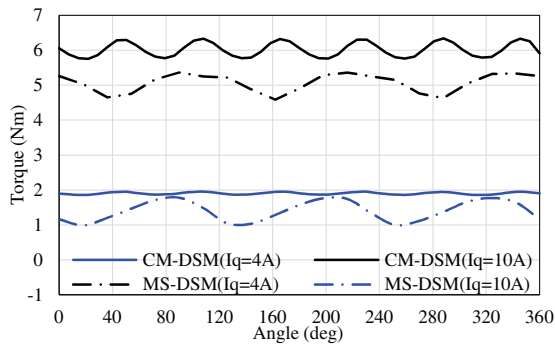


FIGURE 14 Torque characteristics

applications. For instance, cogging torque of the machine describes the initial start torque of wind turbines, and rated output torque of the machine represents its power conversion capability.

The output torque waveforms of the machine under 4 and 10 A current are shown in Figure 14. It can be found that the machine with claw-shaped structure could achieve lower torque ripple under any current condition. It indicates that comparing with the machine without 3D complementary structure, the average torque of CM-DSM is not improved evidently when the DC excitation current is set as 4A, and the average torque only increases when the excitation current comes to 10A. This indicates that the proposed machine has better electrical-mechanical

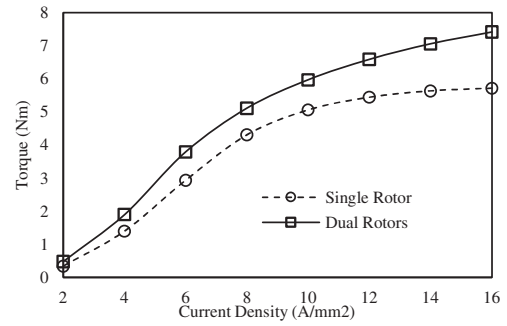


FIGURE 15 Torque characteristics at different excitation with/without complementary rotor

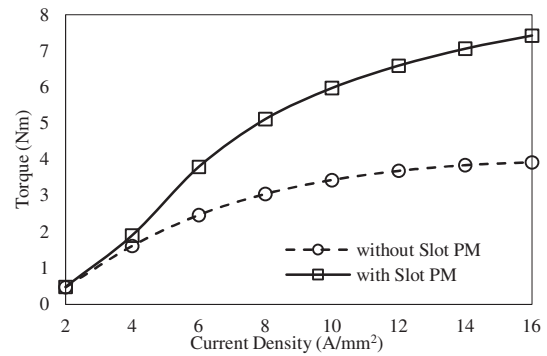


FIGURE 16 Torque characteristics at different excitation with/without auxiliary PMs

conversion capability than the conventional one at heavy load situation.

Furthermore, the torque capability of the machine under different current density is also tested and compared, which is shown in Figure 15. Both the calculation results in Figures 14 and 15 indicate that the average torque of machines with 3D complementary structure could be improved at relatively heavy load situation.

Figure 16 compares the average torque of the proposed machine with or without slot-opening auxiliary PMs, indicating that the machine without auxiliary PM tends to be saturated easily and the output torque is limited as well.

Figure 17 presents the simulation results of the inductance of phase A, including the self-inductance and mutual inductance.

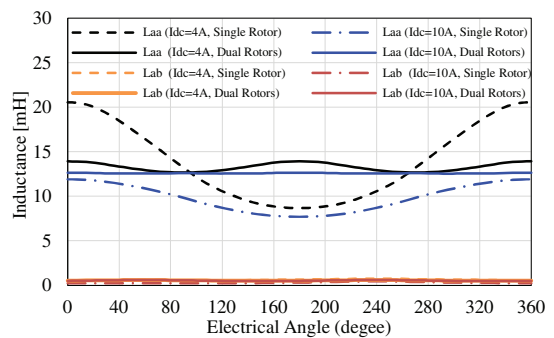


FIGURE 17 Inductance of the proposed CM-DSM

TABLE 6 Comparison results of CM-DSM and MS-DSM machines

	CM-DSM	MS-DSM [7]
Diameter	120 mm	120 mm
Stack length	60 mm	60 mm
Rated speed	1200 rpm	1200 rpm
Rated torque	5.98 Nm	5.06 Nm
Torque ripple	7.05%	15.49%
Induced voltage (phase to phase)	40 V	35 V
DC resistance	0.357 ohm	0.473 ohm
Phase resistance	0.2 ohm	0.158 ohm
Copper loss	95.79 W	86.74 W
Iron loss	35 W	40 W
Output power	750 W	626 W
Efficiency	85.15%	83.16%

The result shows that thanks to the modular stator design, the mutual inductances between different phases are so small that could be neglected, which means that each phases of the machine could be functioned separately.

Table 6 compares the electromagnetic performance of the proposed CM-DSM machine and the conventional MS-DSM machine proposed in [7]. According to Table 6, it could be found that compared with conventional MS-DSM, the proposed CM-DSM generator could achieve higher power capability and lower torque ripple.

The dynamic cogging torque characteristics of CM-DSM and MS-DSM are shown in Figure 18. It shows that the CM-DSM achieves much lower cogging torque than MS-DSM, and the results of 3D and 2D model agree well with each other. Figure 18b presents the dynamic torque under rated current. It can be found that CM-DSM could achieve lower torque ripple and higher output torque. The results of the 3D and 2D models in this condition also agree well with each other.

6 | CONCLUSION

This paper proposed a claw-shaped modular stator doubly salient machine (CM-DSM) with 3D complementary structure for wind power application. Considering the special structure of the machine, 2D equivalent model is proposed to replace 3D model, and the results verified the effectiveness of the equivalent model. The main contribution of this paper lies in the employment of the 3D complementary structure integrated with slot auxiliary PMs on the DCE modular stator machine. Some conclusions can be drawn as follows:

1. Comparing with MS-DSM, thanks to the 3D complementary structure, the voltage-regulation capability of the machine is improved, indicating that the proposed structure has better flux-regulation capability.
2. The output torque of the proposed CM-DSM is increased by 20% at rated current situation after design optimization,

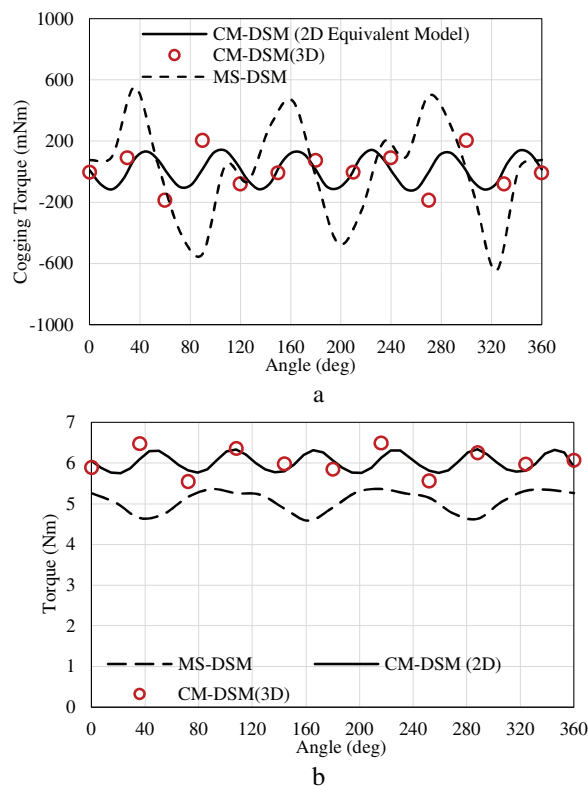


FIGURE 18 Dynamic torque comparison at rated current: (a) cogging torque comparison, (b) output torque comparison

and the saturation current density can be improved from $800\text{A}/\text{mm}^2$ to $1400\text{A}/\text{mm}^2$. Torque ripple of the machine is also reduced from 15.49% to 7.05%.

3. Furthermore, the auxiliary PMs relieved the DC-saturation issue effectively, and the output torque can be increased by 41.6% at rated current excitation.

ACKNOWLEDGEMENTS

This work was supported by the National Natural Science Foundation of China under Project 52077187 and in part by the Research Grant Council of the Hong Kong Government under Project PolyU 152143/18E and PolyU 152109/20E.

ORCID

Zhengbao Li  <https://orcid.org/0000-0001-5727-8773>

REFERENCES

1. Li, H., Chen, Z.: Overview of different wind generator systems and their comparisons. *IET Renewable Power Gener.* 2(2), 123–138 (2008)
2. Wang, Q., Niu, S.: Overview of flux-controllable machines: Electrically excited machines, hybrid excited machines and memory machines. *Renewable Sustainable Energy Rev.* 68, 475–491 (2017)
3. Lee, C.H.T., Chau, K.T., Liu, C.: Design and analysis of a dual-mode flux-switching doubly salient DC-field magnetless machine for wind power harvesting. *IET Renewable Power Gener.* 9(8), 908–915 (2015)
4. Cheng, M., et al.: Overview of stator-permanent magnet brushless machines. *IEEE Trans. Ind. Electron.* 58(11), 5087–5101 (2011)

5. Zhu, Z.Q.: Switched flux permanent magnet machines—Innovation continues. In: 2011 International Conference on Electrical Machines and Systems, pp. 1–10. IEEE (2011)
6. Fan, Y., Chau, K.T., Niu, S.: Development of a new brushless doubly fed doubly salient machine for wind power generation. *IEEE Trans. Magn.* 42(10), 3455–3457 (2006)
7. Zheng, M., et al.: A novel modular stator hybrid-excited doubly salient synchronous machine with stator slot permanent magnets. *IEEE Trans. Magn.* 55(7), 1–9 (2019)
8. Ding, W., et al.: Design consideration and evaluation of a 12/8 high-torque modular-stator hybrid excitation switched reluctance machine for EV applications. *IEEE Trans. Ind. Electron.* 64(12), 9221–9232 (2017)
9. Zhao, W., et al.: Design and analysis of a new modular linear flux-reversal permanent-magnet motor. *IEEE Trans. Appl. Supercond.* 24(3), 1–5 (2014)
10. Wang, D., Wang, X., Du, X.: Design and comparison of a high force density dual side linear switched reluctance motor for long rail propulsion application. *IEEE Trans. Magn.* 53(6) 1–1 (2017)
11. Sheng, T., Niu, S.: Design of doubly complementary stator-PM machine with high magnet utilization factor for low-cost applications. *IEEE Trans. Energy Convers.* 33(2), 567–575 (2018)
12. Niu, S., et al.: A novel axial-flux-complementary doubly salient machine with boosted PM utilization for cost-effective direct-drive applications. *IEEE Access* 7, 145970–145977 (2019)
13. Cao, R., Huang, W., Cheng, M.: A new modular and complementary double-sided linear flux-switching permanent magnet motor with yokeless secondary. In: 2014 17th International Conference on Electrical Machines and Systems (ICEMS), pp. 3648–3652. IEEE (2014)
14. Lee, C.H.T., et al.: Design and analysis of a new multitoothed magnetless doubly salient machine. *IEEE Trans. Appl. Supercond.* 24(3), 1–4 (2014)
15. Yubin, W., et al.: Design and analysis of a HTS flux-switching machine for wind energy conversion. *IEEE Trans. Appl. Supercond.* 23(3), 5000904–5000904 (2013)
16. Zhao, X., et al.: Design of a new relieving-DC-saturation hybrid reluctance machine for fault-tolerant in-wheel direct drive. *IEEE Trans. Ind. Electron.* 67(11), 9571–9581 (2020)

How to cite this article: Li, Z., Niu, S.: Design and analysis of a novel claw-shaped modular stator relieving-DC-saturation doubly salient machine with 3D complementary magnetic circuit. *IET Renew. Power Gener.* 15, 2052–2062 (2021).
<https://doi.org/10.1049/rpg2.12224>